A Novel Bio-Inspired Texture Descriptor based on Biodiversity and Taxonomic Measures

Steve Tsham Mpinda Ataky[a], Alessandro Lameiras Koerich[a]

[a]*École de Technologie Supérieure, Université du Québec*
1100, rue Notre-Dame Ouest, H3C 1K3, Montréal, QC, Canada

Abstract

Texture can be defined as the change of image intensity that forms repetitive patterns, resulting from physical properties of the object's roughness or differences in a reflection on the surface. Considering that texture forms a complex system of patterns in a non-deterministic way, biodiversity concepts can help texture characterization in images. This paper proposes a novel approach capable of quantifying such a complex system of diverse patterns through species diversity and richness and taxonomic distinctiveness. The proposed approach considers each image channel as a species ecosystem and computes species diversity and richness measures as well as taxonomic measures to describe the texture. The proposed approach takes advantage of ecological patterns' invariance characteristics to build a permutation, rotation, and translation invariant descriptor. Experimental results on three datasets of natural texture images and two datasets of histopathological images have shown that the proposed texture descriptor has advantages over several texture descriptors and deep methods.

Keywords: Texture Classification, Texture Characterization, Species Richness, Taxonomic Distinctiveness, Phylogenetic Indices, Species Abundance.

1. Introduction

Texture is an important descriptor that has been used in several image analysis [1] and computer vision [2] applications, such as agriculture [3], recognition of facial expressions [4], object recognition [5], medical image analysis [6], music genre classification [7], remote sensing [8], material [9] and surface [10] recognition, and so on. Texture analysis aims at establishing the neighborhood relationship of the texture elements and their position concerning the others (connectivity),

the number of elements per spatial unit (density), and their regularity (homogeneity). Texture descriptors developed to characterize image textures by and large fall into statistical methods and geometric methods [11]. The statistical methods aim to discover to which extent some image properties related to its texture may be distributed and derive numerical measures. In contrast, the geometric methods investigate the periodicity in an image and characterize a texture with its relative spectral energy.

Several approaches for texture information extraction have been developed in the last three decades such as gray-level co-occurrence matrix (GLCM) [12], Haralick descriptors [13], local binary patterns (LBP) [14], wavelet transform [15], Markov random fields [16], Gabor texture discriminator [17], local phase quantization [18], local tera pattern [19], binarized statistical image features [20], and fractal models [21]. A review of most of these approaches can be found in Simon and Uma [22] and Liu et al. [23]. Researchers have recently focused on convolutional neural networks (CNNs) due to their effectiveness in object detection and recognition tasks. However, the shape information extracted by CNNs is of minor importance in texture analysis [24]. Andrearczyk and Whelan [24] develop a simple texture CNN (T-CNN) architecture for analyzing texture images that pools an energy measure at the last convolution layer and discards the overall shape information analyzed by classic CNNs. Despite the promising results, the trade-off between accuracy and complexity is not so favorable. Other texture CNN architectures have also achieved moderate performance on texture classification [25–27].

Even if most of the texture descriptors previously mentioned have proven to be discriminative for texture classification, they do not exploit the color information that may exist in natural and microscopic images. To overcome such a limitation, Qi et al. [28] introduced an approach that encodes cross-channel texture correlation and an extension of LBP that incorporates color information. Nsimba and Levada [29] have also exploited color information for texture classification. They presented a novel approach to compute information theory measures that capture important textural information from a color image. The accuracy achieved by both approaches is very promising and shows the importance of using color information for texture characterization.

This paper introduces a novel bio-inspired texture (BiT) descriptor based on biodiversity measurements (species richness and evenness) and taxonomic distinctiveness. Ecology primarily exploits these concepts considering patterns in ecosystems. In this work, textural patterns are considered an ecosystem, where both the biodiversity measurements and taxonomic indices are

computed and quantified. Azevedo et al. [30] and de Carvalho Filho et al. [31] have used some taxonomic indices for the diagnosis of glaucoma on retinographs and lung nodules, respectively. It is also worth mentioning that these works employed taxonomic indices to extract features of specific types of medical images, such as glaucoma and lung nodules. The bio-inspired texture descriptor proposed in this paper is a general texture descriptor that can characterize texture information on various texture images. Furthermore, the proposed approach also exploits color information [28, 29]. We represent and describe biodiversity as the interaction of pixels with their neighborhood within each image channel (R, G, or B) as well as on a single RGB image. Besides, taxonomic indices and species diversity and richness measures on which the novel BiT descriptor relies are of an underlying use as they capture the all-inclusive behavior of texture image patterns. They capture the intrinsic properties of the whole ecosystem, which forms a non-deterministic complex system.

The main contribution of this paper is a novel bio-inspired descriptor that exploits species diversity and richness and taxonomic distinctiveness to build a representation for texture classification. More specifically, the contributions are: (i) modeling each channel of a color image as an ecosystem; (ii) a novel bio-inspired texture (BiT) descriptor that combines measurements of species diversity and richness and taxonomic distinctiveness; (iii) the BiT descriptor is invariant to scale, translation and permutation; (iv) the BiT descriptor is easy to compute and has low computational complexity; (v) the BiT descriptor is a generic texture descriptor that performs well on different categories of images, such as natural textures and medical images.

The organization of the remainder of this paper is as follows. Section 2 presents the proposed bio-inspired texture descriptor based on biodiversity measurements and taxonomic distinctiveness. Section 3 describes a baseline approach to classify texture images, which is used to assess the performance of the proposed BiT descriptor and to compare its performance with other classical texture descriptors. Section 4 presents the datasets and the experimental protocol. Experimental results, comparison with other texture descriptors and deep approaches, and discussion are presented in Section 5. Finally, the conclusions are stated in the last section.

2. Biodiversity and Taxonomic Distinctiveness

Diversity is a term often used in ecology, and the purpose of diversity indices is to describe the variety of species present in a community or region [32]. Community is defined as a set of

species that occurs in a particular place and time. Statistical studies frequently use quantitative measurements of variability such as mean and variance, while diversity indices describe qualitative variability. Diversity is measured through two variants: (i) species richness, which represents the number of species of a given region; (ii) relative abundance, which refers to the number of individuals of a given species in a given region) [33]. However, diversity cannot be measured only in terms of abundance and species richness. It requires the inclusion of a phylogenetic parameter [34]. Phylogeny is a biology branch responsible for studying the evolutionary relationships between species to determine possible common ancestors. The combination of species abundance with phylogenetic proximity to generate a diversity index is denoted as taxonomic diversity. Taxonomy is the science that deals with classification (creating new taxa), identification (allocation of lineage within species), and nomenclature.

A phylogenetic tree combined with phylogenetic diversity indices compares behavior patterns between species in different areas in biology. Phylogenetic indices (biodiversity and taxonomic indices) can characterize texture due to their potential in describing patterns of a given region/image, regardless of forming a non-deterministic complex system. The richness of details obtained with each indices group is essential for the composition of the descriptors proposed in this paper. We state that these indices are suitable for describing textures due to their ability to analyze the diversity between species in a region.

2.1. Images as Ecosystems

We assume that an image is an abstract model of an ecosystem where: (i) gray levels of pixels in an image correspond to the species in an ecosystem; (ii) pixels in an image correspond to the individuals in an ecosystem; (iii) the number of different gray levels in an image corresponds to species richness in an ecosystem; (iv) the number of distinct gray levels in a specific region of an image corresponds to species abundance in an ecosystem. Another factor is that both the patterns in an ecosystem and the patterns in texture images form a non-deterministic system. Figure 1 illustrates an ecosystem with three species, six individuals of white species, five individuals of gray species, and five individuals of black species.

2.2. Biodiversity and its Measurements

Biodiversity is defined as the variety within and among life forms on an ecosystem or a site. Biodiversity is measured as a combination of richness and evenness across species [33]. Diversity
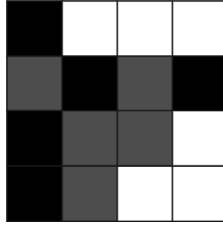
Figure 1: A gray-level image as an abstract model of an ecosystem of three species (three gray-levels): white (6 individuals), gray (5 individuals) and black (5 individuals).

can represent variation in several forms, such as genetic, life form, and functional group. It is worthy of mention that diverse communities are often a sign of fragmented sites where much of species richness is contributed by disturbance species [33]. Different objective measures have been proposed as a means to measure biodiversity empirically. The fundamental idea of a diversity index is to quantify biological variability, which, in turn, can be used to compare biological entities composed of direct components, in whether space or time [35]. Biodiversity can be expressed or monitored at different scales and spaces: alpha diversity, beta diversity, and gamma diversity. Jost [36] presents more details on these three types of indices.

2.2.1. Diversity Measures

Diversity measurements rely on three assumptions [32]: (i) all species are equal – richness measurement makes no distinctions among species and treats the species that are exceptionally abundant in the same way as those extremely rare; (ii) all individuals are equal – there is no distinction between the largest and the smallest individual; however, in practice, the least animals can often escape, for instance, by sampling with nets. This does not necessarily apply to taxonomic and functional diversity measures;; (iii) species abundance is recorded using appropriate and comparable units.

We can translate such assumptions to our abstract model as: (i) all gray levels are equal – richness measurement makes no distinctions among gray levels and treats the gray levels that are exceptionally abundant in the same way as those significantly less represented; In other words, all gray levels within an image are taken into account for further calculation, regardless of how non-representative some of them are; (ii) all pixel values are equal – there is no distinction between the largest and the smallest pixel value; (iii) gray-level abundance has to be recorded using appropriate and comparable units such as the intensity.

Some alpha diversity measures, including measures of richness, dominance, and evenness [37]

are described as follows. They represent the diversity within a particular ecosystem: the richness and evenness of individuals within a community. All these indices are computed on a gray-scale image of dimension n and m, which is denoted as $\mathbf{I}_{m \times n}$.

Margalef's (d_{Mg}) [32, 38] and **Menhinick's** (d_{Mn}) [39] **diversity index** are both the ratio between the number of species (S) and the total number of individuals in the sample (N):

$$d_{\mathrm{Mg}} = \frac{S - 1}{\ln N} \tag{1}$$

$$d_{\mathrm{Mn}} = \frac{S}{N} \tag{2}$$

where, S and N denote the number of gray levels and the total number of pixels in an image, respectively.

Berger-Parker dominance (d_{BP}) [40] is the ratio between the number of individuals in the most abundant species (N_{max}) and the total number of individuals in the sample:

$$d_{\mathrm{BP}} = \frac{N_{max}}{N} \tag{3}$$

where N_{max} denotes the most frequent gray level in an image.

Fisher's alpha diversity metric (d_{F}) [37, 41] denotes the number of operational taxonomic units, that is, groups of closely related individuals and it is defined as:

$$d_{\mathrm{F}} = \alpha \ln \left(1 + \frac{N}{\alpha} \right) \tag{4}$$

where α is approximately equal to the number of gray levels represented by a single pixel.

Kempton-Taylor index of alpha diversity (d_{KT}) [42] measures the interquartile slope of the cumulative abundance curve, where n_r is the number of species with abundance R; R_1 and R_2 are the 25% and 75% quartiles of the cumulative species curve; n_{R_1} is the number of individuals in the class where R_1 falls; n_{R_2} is the number of individuals in the class where R_2 falls:

$$d_{\mathrm{KT}} = \frac{\frac{1}{2} n_{R_1} + \sum_{R_1+1}^{R_2-1} n_r + \frac{1}{2} n_{R_2}}{\log \frac{R_2}{R_1}} \tag{5}$$

6

where n_r denotes the number of gray levels with abundance R; S is the number of gray levels in the image; R_1 and R_2 are the 25% and 75% quartiles of the cumulative gray scale curve; n_{R_1} is the number of pixels in the class where R_1 falls; n_{R_2} is the number of pixels in the class where R_2 falls.

McIntosh's evenness measure (e_M) [43] is the ratio between the number of individuals in the i-th species and the total number of individuals, and the number of species in the sample:

$$e_M = \sqrt{\frac{\sum_{i=1}^{S} n_i^2}{(N - S + 1)^2 + S - 1}} \tag{6}$$

where n_i denotes the number of pixels of the i-th gray-level (the summation is over all gray levels).

Shannon-Wiener diversity index (d_{SW}) [37] is defined as the proportion of individuals of species i in terms of species abundance (S):

$$d_{SW} = -\sum_{i=1}^{S} (p_i \, log_e \, p_i) \tag{7}$$

where p_i denotes the proportion of pixels with the i-th gray-level.

2.3. Taxonomic Indices

The ecological diversity indices presented in the previous section are based on the richness and abundance of species present in a community. Nevertheless, such indices may be insensitive to taxonomic differences or similarities. With equal species abundances, they measure but the species richness. Assemblages with the same species richness may either comprise species closely related taxonomically or more distantly related [44]

Taxonomic indices consider the taxonomic relation between different individuals in an ecosystem. The diversity thereof reflects the average taxonomic distance between any two individuals, randomly chosen from a sample. The distance can represent the length of the path connecting these two individuals along the branches of a phylogenetic tree [44]. Taxonomic diversity and taxonomic distinctiveness define the relationship between two organisms randomly chosen in an existing phylogeny in a community [34, 45], and they are characterized by three key factors: (i) number of individuals; (ii) the number of species; (iii) the structure of species connection, that is, the number of edges. Furthermore, Gibson et al. [45] also proposed the distinctiveness in-

dex describing the average taxonomic distance between two randomly chosen individuals through the phylogeny of all species in a sample. This distinctiveness may be represented as taxonomic diversity and taxonomic distinctness [35], which is described as follows.

Taxonomic diversity (Δ) [34] includes aspects of taxonomic relatedness and evenness. In other words, it considers the abundance of species (number of different gray levels) and the taxonomic relationship between them, and whose value represents the average taxonomic distance between any two individuals (pixels), chosen at random from a sample.

$$\Delta = \frac{\sum_{i=0}^{S} \sum_{i<j}^{S} w_{ij} x_i x_j}{\dfrac{N(N-1)}{2}} \tag{8}$$

where x_i, x_j, and w_{ij} represent the number of pixels that have the i-th gray-level in the image, the number of pixels that have the j-th gray-level in the image, and the 'distinctness weight' (distance) given to the path length linking pixels i and j in the hierarchical classification, respectively, and $i, j = 0, \ldots, S$.

Taxonomic distinctiveness (Δ^*) is a measure of pure taxonomic relatedness. It represents the average taxonomic distance between two individuals (pixels), constrained to pertain to different species (gray levels).

$$\Delta^* = \frac{\sum_{i=0}^{S} \sum_{i<j}^{S} w_{ij} x_i x_j}{\sum \sum_{i<j} x_i x_j} \tag{9}$$

Different ecological studies, particularly large-scale ones, employ species richness as a measure of biodiversity. Nevertheless, species richness as the sole reflection of biodiversity can present limitations as all species are treated equally without considering phylogenetic relationships. The literature shows that phylogenetic relationships are one of the most important factors, as they determine, for example, the extinction of species. Thus, phylogenetic information may be a better indicator of the preservation value than just the species richness. The studies that verify the distance relationship between the pairs of species are based on a distance matrix computed for all species of a community. In ecology, this distance matrix relies on either functional or morphological differences [46], on the length of the branches of the phylogenetic relationships based on molecular data [47]. Accordingly, if the branches' length is unknown, such distances rely

on the number of nodes that separate each pair of species [48]. The distance matrix values can be interpreted as the distinctness between each pair of species or between each particular species vis-à-vis all others [46]. The following indices are based on the distances between pairs of species.

Sum of Phylogenetic Distances (s_{PD}) represents the sum of phylogenetic distances between pairs of species.

$$s_{PD} = \left(\frac{S(S-1)}{2} \right) \frac{\sum\limits_{i<j^2} \sum ij^a i^a j}{\sum\limits_{i<j^a} \sum i^a j} \tag{10}$$

where i and j denote two distinct gray levels, and a is the number of pixels that have such gray levels.

Average Distance from the Nearest Neighbor (d_{NN}) [49] represents the average distance to the nearest taxon.

$$d_{NN} = \sum_{i}^{S} \min\left(d_{ij} a_i\right) \tag{11}$$

where d_{ij} is the distance between gray levels i and j.

Extensive Quadratic Entropy (e_{EQ}) represents the sum of the differences between gray levels.

$$e_{EQ} = \sum_{i \neq j}^{S} d_{ij} \tag{12}$$

Intensive Quadratic Entropy (e_{IQ}) represents the number of species and their taxonomic relationships. It aims at establishing a possible link between the diversity indices and the biodiversity measurement indices. Thus, expressing the average taxonomic distance between two species chosen at random, the relationships between them influence the entropy, unlike other diversity indices.

$$e_{IQ} = \frac{\sum\limits_{i \neq j}^{S} d_{ij}}{S^2} \tag{13}$$

Total Taxonomic Distinctness (d_{TT}): represents the average phylogenetic distinctiveness added across all species (gray levels).

$$d_{TT} = \sum i \frac{\sum\limits_{i \neq j}^{S} d_{ij}}{S-1} \tag{14}$$

9

It is worth noting that Equations 1 to 9 are based on species richness, abundance and evenness, whereas Equations 10 to 14 are based on the pairwise distance between pairs of species. All measurements described in Equations 1 to 14 can then be computed from an image – in this paper, from each channel of a color image – and all of them result in scalar values, which can be further normalized within the interval $[0, 1]$. These scalars are then concatenated to form a d-dimensional feature vector of scalars, which we named BiT descriptor.

The taxonomic indices require a taxonomic tree to compute species' joint dissimilarity (different gray levels) or pairwise distances between species (different gray levels). The topological distance, defined as the number of edges between two species in the Linnaean taxonomic tree, is the full phylogenetic tree's cumulative branch length. An example of a taxonomic tree and its species distance matrix is shown in Figure 2.
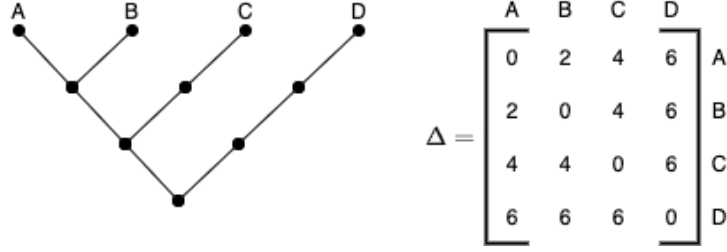

Figure 2: Generic example of taxonomic tree for four species (A, B, C, and D) and its respective distance matrix. This matrix shows how cumulative branch length, which corresponds to taxonomic distances, is calculated. Image adapted from Ricotta [50].

Based on the example mentioned above (Figure 2), we can derive an instance of the taxonomic tree and its corresponding distance matrix of gray levels (Figure 3). We have represented the taxonomic tree as a matrix, where the distance between two pixels represents the distance between two species. The division of species in the rooted tree shows the phylogenetic relationship between ancestor species. Such a division allows computing indices connecting diversity, richness, and parenthood between them. Furthermore, a dendrogram can describe the evolutionary relationships between species: the parenthood relationship between gray levels, where the leaves represent the species and the internal nodes represent the common ancestors to the species. This allows establishing an evolutionary connection between the gray levels (species) [51], which, in this work, relies on the intrinsic proprieties of the texture present in an image. Thus, the division of an image or a patch for generating a dendrogram should be based on the parenthood, that is, the similarity between pixels.

Figure 3 illustrates the process of division performed in a region of an image to assemble a
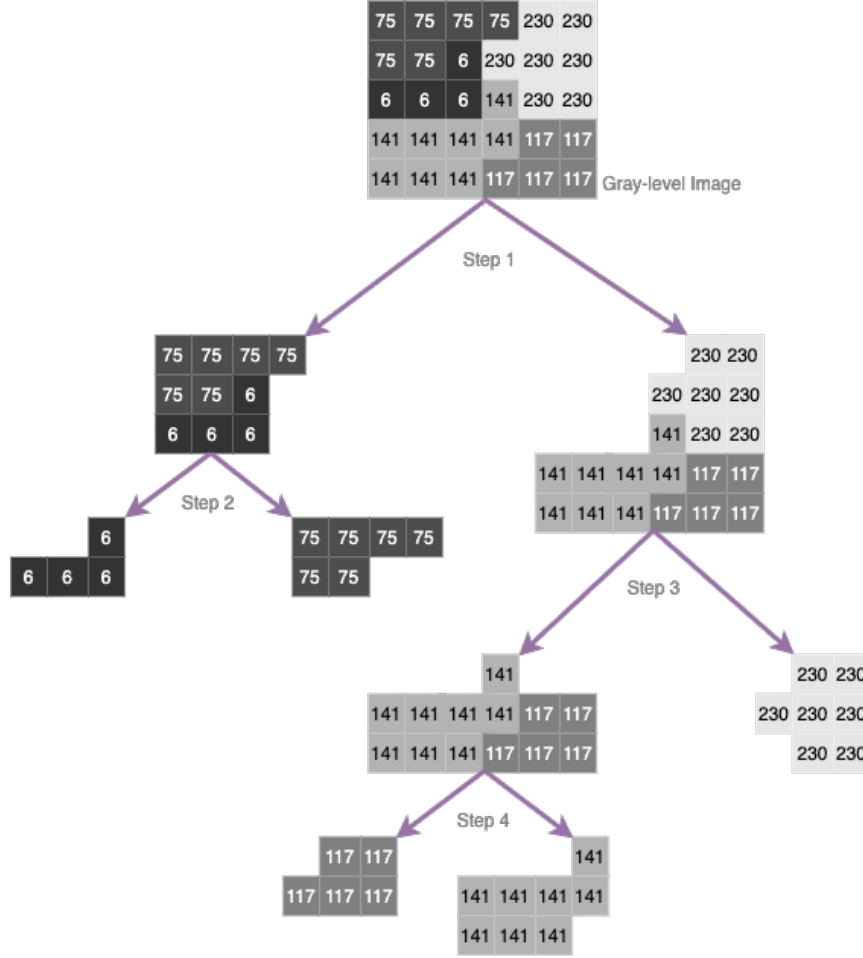
Figure 3: Construction of a phylogenetic tree for computing the taxonomic indexes. In each iteration (step) the image is divided based on species (gray levels). The average species value is used as threshold at each step.

phylogeny tree (dendrogram) based on the similarity between pixels (gray levels) for computing the taxonomic indexes. In this case, some iterations are needed to divide the original region/image until a single gray level remains on each leaf. The division is carried out based on a threshold, which splits a region into two parts, each containing pixels of gray levels above (right) and below (left) the threshold, successively. The threshold can be the average gray-level of all pixels.

From the original image, in the first iteration (step 1), gray levels 6 and 75 (left) are below the threshold, whereas gray levels 117, 141, and 230 (right) are above the threshold. The second iteration (step 2) splits the left part resulting from step 1, that is, gray levels 6 (left) and 75 (right), into two parts. Since there are single gray levels in each region resulting from step 2, these regions become leaves. The third iteration (step 3) separates the right part resulting from step 1 into two parts: pixels of gray levels 141 and 117 go to the left, while pixels of gray-level

230 to the right. Finally, the fourth iteration (step 4) separates the left part from step 3 into two parts: pixels of gray levels 141 and 117. Figure 4 illustrates the rooted tree, the dendrogram, and the respective species (gray levels) as well as their characteristics.
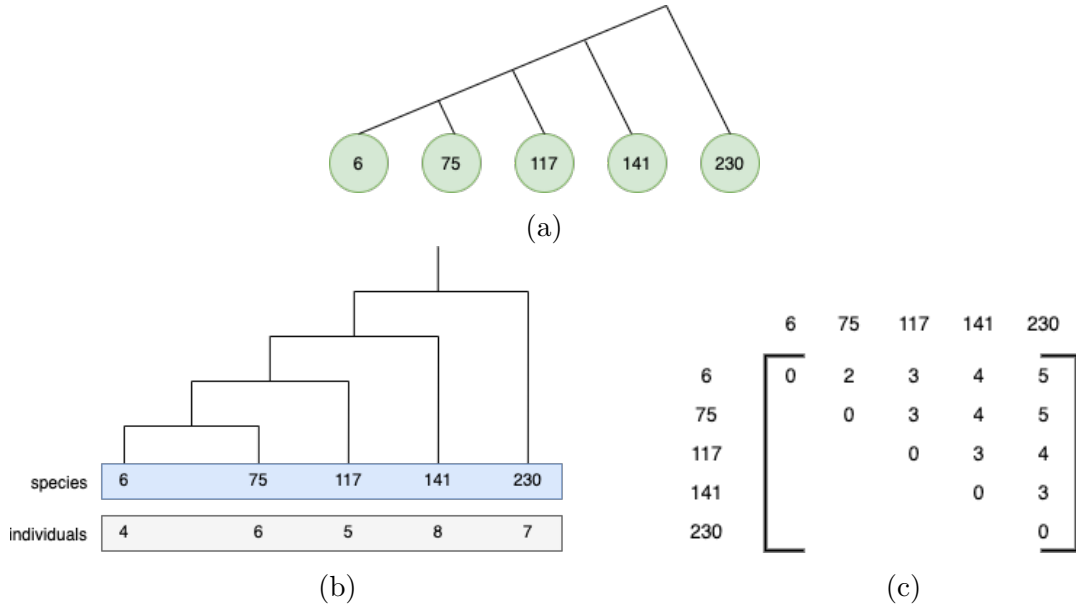

Figure 4: Example of (a) rooted tree; (b) a dendrogram; (c) and the respective distance matrix of gray levels computed from the image in Figure 3. Note that (a) and (b) are equivalent. The dendrogram allows computing the phylogenetic indexes to infer the phylogenetic relationship between existing gray levels in the original image. Therefrom, the taxonomic indexes are likewise computed.

2.4. Properties of BiT Descriptors

For many applications, a texture descriptor must have important properties such as invariance to rotation, translation, and scale. Furthermore, the descriptor should be easy to calculate.

The diversity indices based on species richness measure properties directly related to species, such as their relative abundance and evenness. These measurements are invariant to in-plane rotations and scale (because the true essence of pattern is invariance). The fundamental idea of diversity indices is to quantify biological variability, which, in turn, can be used to compare biological entities composed of direct components, whether space or time [35]. Biodiversity can be expressed or monitored at different scales and spaces. It is assumed that all species are equal, meaning that richness measurement makes no distinctions among species and treats the species that are exceptionally abundant in the same way as scarce species. All individuals are equal, meaning no distinction between the largest and the smallest individual [32].

In our abstract model, these assumptions may be expressed as pixels of any gray level are

12

equal. Therefore, richness measurement makes no distinctions among gray levels and treats pixels that are exceptionally abundant in the same way as pixels that are extremely less represented. In other words, pixels of all gray levels present in an image are taken into account for further calculation, regardless of how non-representative some are; and all pixel values are equal, that is, there is no distinction between the largest and the smallest pixel value.

In ecology, a pattern is subject to how form remains invariant to changes in measurement. Some patterns retain the same shape after uniformly stretching or shrinking the scale of measurement. The rotational invariance in the ecological pattern has been stated by Frank and Bascompte [52], being the most general way to understand commonly observed patterns. From there, species abundance distributions provide a transcendent example, in which the maximum entropy and neutral models can succeed in some cases because they derive from invariance principles. Likewise, as presented by Daly et al. [53], diversity is invariant to the species abundance vector's permutation. Rousseau et al. [54] emphasizes that there is a one-to-one correspondence between abundance vectors and Lorenz curves. Consequently, abundance vectors can be partially ordered by the Lorenz order, which is permutation-invariant (rotation) and scale-invariant.

Therefore, the BiT descriptor combines statistical and structural approaches and takes advantage of ecological patterns' invariance characteristics to permutation, rotation, and scale by combining species richness, abundance, evenness, and taxonomic indices.

2.5. BiT and other Texture Descriptors

The BiT descriptor shares some characteristics of both GLCM [12] and LBP [14] descriptors in the sense that BiT also characterizes textures based on second-order statistical properties, which involves comparing pixels and determining how a pixel at a specific location relates statistically to pixels at different locations.

In ecology, taxonomic indices are approximations of second-order statistics at the species level. These indices are based on group analysis, thus enabling a behavioral exploration of the neighborhood of regions displaced from a reference location. Given a distance measurement between pairs of species (pairs of pixels of different gray levels), a classical approach to solving the phylogeny issue can be finding a tree that predicts the observed set of adjoining distances. Such distances are represented in a matrix that indicates the existing phylogenetic distance, reducing it to a simple table of pairwise distances [44, 51].

Furthermore, the BiT descriptor also shares some characteristics of Gabor filters [17]. Gabor

filters explore different periodicities in an image and attempt to characterize a texture at these different periodicities. This analysis is confined to the adjacent neighborhoods of the individual pixels. These within-neighborhood periodicity properties can be used to recognize texture differences between the different regions. Accordingly, phylogenetic trees combined with diversity indices are used in biology to compare behavioral patterns between species in different areas and within-neighborhood. Besides, diversity indices based on species richness are of an underlying use when defining an all-inclusive behavior of an ecosystem, forming a non-deterministic complex system.

3. Case Study

This section presents how the proposed bio-inspired texture descriptor can be integrated with image processing and machine learning algorithms for classification tasks. The proposed classification scheme is structured into five stages: image channel splitting, pre-processing, feature extraction, training, and classification. Figure 5 shows an overview of the proposed scheme. Algorithm 1 integrates the first three steps, and it receives an RGB image as input and provides a d-dimensional feature vector of BiT descriptors. An implementation of this algorithm is available as a Python module[1]. The five stages are described as follows.
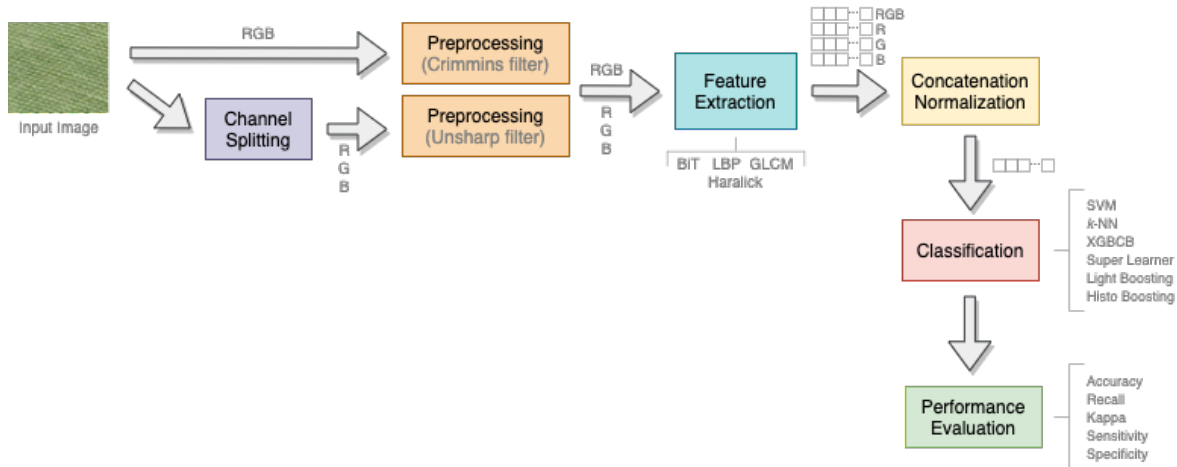

Figure 5: An overview of the proposed scheme to evaluate the BiT descriptor and compare it with other texture extractors.

---

[1]https://github.com/stevetmat/BioInspiredFDesc. The Python class **BiT**(*image, b_feat = True, t_feat = True, unsharp_filter = True, crimmins_filter = True, normalization = True*) generates a 56-dimensional feature vector.

Channel Splitting:. Besides the original RBG image, each image channel (R, G, B) is considered a separate input. Notwithstanding the texture descriptors presented in Section 1 have shown a discriminative ability to classify texture patterns, their performance on natural and microscopic images is bounded because they are applied only to gray-scale images. Thus, they do not exploit color information. The key reason behind splitting channels is that we aim to capture the textural information of color images based on the principle that most ecosystems work in a cause-effect relationship. Such a relationship implies that when one resource is added or lost, it affects the entire ecosystem. Some of the most marked temporal/spacial fluctuations in species abundances are linked to this cause-effect relationship [55]. Therefore, we characterize the biodiversity in an image by a set of local descriptors generated from the interaction between a pixel and its neighborhood in each channel (R, G, B) and in the RGB image.

Pre-Processing:. It consists of an unsharp filter to highlight image characteristics and a Crimmins filter to remove speckles [56]. Unsharp filter is applied to each image channel and Crimmins filter is applied to the RGB image to improve their quality for the feature extraction step.

Feature Extraction:. After the pre-processing step, the images undergo feature extraction, which looks for informative and discriminative characteristics within the images. Images are then represented by several measurements organized in feature vectors. From each image, we extract: biodiversity measurements (Equations 1 to 7) and taxonomic indices (Equations 8 to 14).

Classification:. the final step of the proposed scheme consists of classifying images in different classes, using a shallow approach where feature vectors are used to train different classification algorithms as detailed in Section 4. The results obtained are presented and discussed in Section 5.

4. Experimental Protocol

In this section, we present the datasets used to assess the performance of the proposed BiT descriptor, which includes natural texture images and histopathological images (HIs) and the experimental protocol to evaluate the proprieties of the BiT descriptor and its performance on classification tasks. We compare the BiT descriptor's performance with classical texture descriptors such as LBP, GLCM, and Haralick. It is worthy of mentioning that our contribution relies on the combination of biodiversity measurements and taxonomic indices to build a discriminative descriptor capable of efficiently classifying textures.

Algorithm 1: Feature_Extraction_Procedure

Description: Compute BiT descriptor
Input   : A RGB image $\mathbf{I}_{m \times n \times 3}$
Output   : A d-dimensional feature vector $\mathbf{x}$
1. Separate the RGB image $\mathbf{I}$ in channels $\mathbf{I}^{\mathrm{R}} = \mathbf{I}[1 \ldots n, 1 \ldots m, 1]$,
  $\mathbf{I}^{\mathrm{G}} = \mathbf{I}[1 \ldots n, 1 \ldots m, 2]$, $\mathbf{I}^{\mathrm{B}} = \mathbf{I}[1 \ldots n, 1 \ldots m, 3]$;
2. Convert $\mathbf{I}$, $\mathbf{I}^{\mathrm{R}}$, $\mathbf{I}^{\mathrm{G}}$, and $\mathbf{I}^{\mathrm{B}}$ to grayscale images $\mathbf{I}^{\mathrm{g}}$, $\mathbf{I}^{\mathrm{Rg}}$, $\mathbf{I}^{\mathrm{Gg}}$, and $\mathbf{I}^{\mathrm{Bg}}$;
3. Apply unsharp filter to $\mathbf{I}^{\mathrm{Rg}}$, $\mathbf{I}^{\mathrm{Gg}}$, and $\mathbf{I}^{\mathrm{Bg}}$;
4. Apply Crimmins filter to $\mathbf{I}^{\mathrm{g}}$;
5. Compute biodiversity measurements (Equations 1-7) and taxonomic indices
  (Equations 8-14) for $\mathbf{I}^{\mathrm{Rg}}$, $\mathbf{I}^{\mathrm{Gg}}$, $\mathbf{I}^{\mathrm{Bg}}$, and $\mathbf{I}^{\mathrm{g}}$;
6. Concatenate the computed measures and indices into a single vector $\mathbf{x}$;
7. Normalize all values of $\mathbf{x}$;
8. Return $\mathbf{x}$;

4.1. Texture Datasets

We use three texture datasets that have already been employed for evaluating texture descriptors such as LBP, GLCM, and Haralick [22]. The Salzburg dataset[2] contains a collection of 476 color texture images of resolution 128×128, captured around Salzburg, in Austria. These images belong to 10 different classes, and 70% of the images are used for training and validating the classification algorithms, while the remaining 30% are used for testing. Figure 6(a) shows some samples from the Salzburg texture dataset.

The Outex_TC_00010_c dataset[3] has a training set consisting of 20 non–rotated color images of each of the 24 classes (480 in total) of illuminant "inca", color counterpart of the original Outex_TC_00010[4] dataset. The test set consists of 3,840 color images of eight orientations (5, 10, 15, 30, 45, 60, 75, and 90 degrees). Figure 6(b) shows some samples from the training set of the Outex dataset.

The KTH-TIPS dataset[5] contains a collection of 810 color texture images of 200×200 pixel of resolution. The images were captured at nine scales, under three different illumination directions and three different poses, with 81 images per class. Seventy percent of images are used for training, while the remaining 30% are used for testing. Figure 6(c) shows some samples from the KTH-TIPS dataset.

---

[2]http://www.wavelab.at/sources/STex/
[3]http://lagis-vi.univ-lille1.fr/datasets/outex.html
[4]http://lagis-vi.univ-lille1.fr/datasets/outex.html
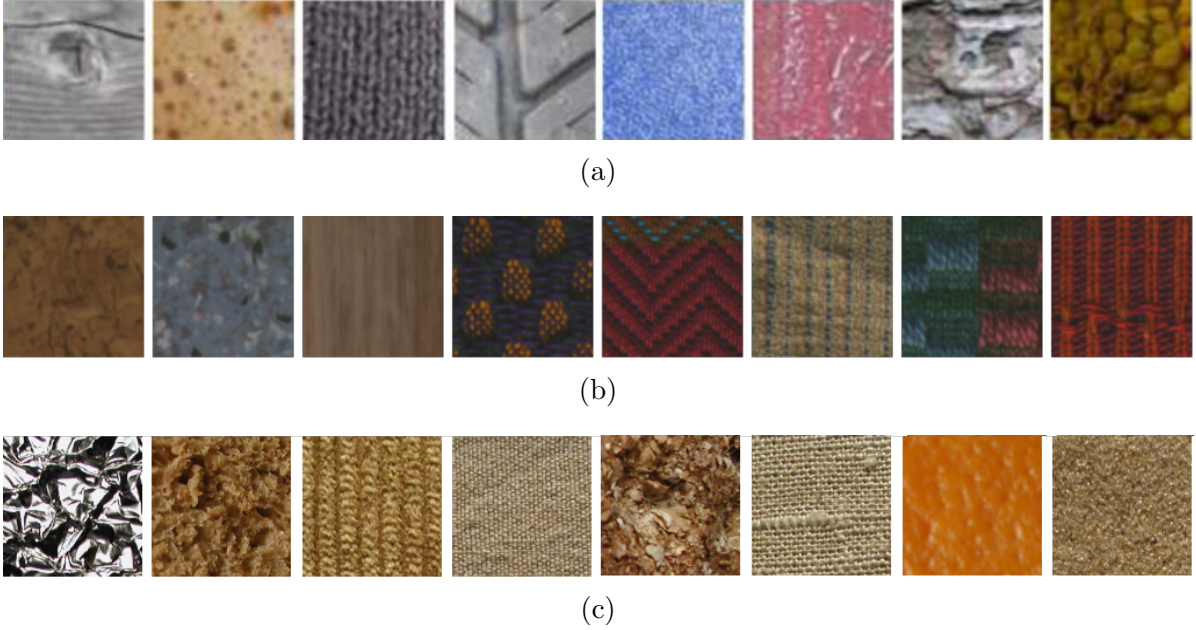[5]https://www.csc.kth.se/cvap/databases/kthtips/download.html

Figure 6: Samples from the texture datasets: (a) Salzburg, (b) Outex_TC_00010_c, and (c) KTH-TIPS.

4.2. Histopathological Image (HI) Datasets

HIs were included in the experiments because they are more challenging than pure texture images since HIs usually have other structures such as nuclei (shape) and variations of tissues (colors) within the same class.

The CRC dataset [57] encompasses colorectal cancer histopathology images of dimension 5,000×5,000 pixels that were cropped into 150×150 patched and labeled according to the structure they contain. Eight types of structures are labeled: tumor (T), stroma (ST), complex stroma (C), immune or lymphoid cells (L), debris (D), mucosa (M), adipose (AD), and background or empty (E). Each structure detailed in the CRC dataset has a specific textural characteristic. Few shape characteristics are found in cell nuclei formation, which has a rounded shape, but with different coloring due to hematoxylin. The total number of images is 625 per structure type, resulting in 5,000 images. Figure 7 shows samples of each class from the CRC dataset. The experiments were performed with stratified 10-fold cross-validation.

The BreakHis dataset [58] is composed of 7,909 microscopic images of breast tumor tissue collected from 82 patients using different magnification factors (40×, 100×, 200×, and 400×). The breast tissues extracted from biopsy usually have some basic structures, such as glands, ducts, and supporting tissue. Comparing a region with a malignant tumor ductal carcinoma, for example, with a region that does not, there will be a difference in texture between them.
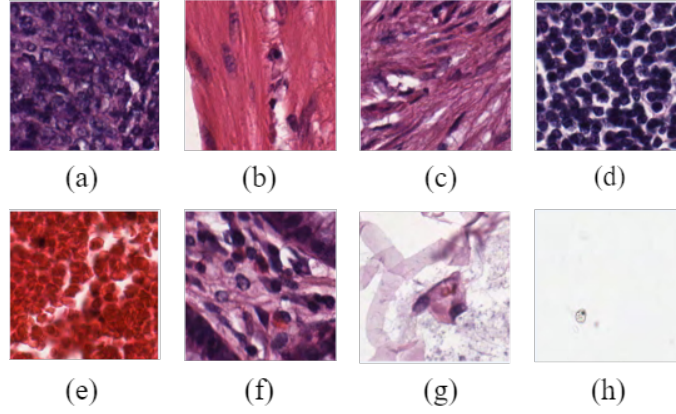
17

Figure 7: Samples of the CRC dataset: (a) tumor, (b) stroma, (c) complex, (d) lympho, (e) debris, (f) mucosa, (g) adipose, (h) empty.

There will be a large presence of nuclei in the region with carcinoma, identified by the purple color of hematoxylin's reaction with its proteins. The nuclei and many cells in a reduced region make the apparent texture to be noisier. In a region without carcinoma, the epithelial tissue is thin and delimits two regions, lumen and stroma, which have different textural characteristics from the excess of epithelial cells. The lumen generally presents itself as a homogeneous and whitish region. Due to its reaction to eosin, the stroma presents a pink and also homogeneous color, with little noise. At this point, a texture descriptor can assist in detecting carcinomas by characterizing a given texture. Nevertheless, the evaluation of types of malignant tumors, that is, differentiation between types of carcinoma on a dataset such as BreaKHis, would need to detect shape to differentiate the papillae from a disorderly cluster of cells, for instance.

The BreakHis dataset contains 2,480 benign and 5,429 malignant samples (700×460 pixels, 3-channel RGB, 8-bit depth in each channel, PNG format). We used hold-outs with repetition, where 70% of samples are used for training and 30% of samples are used for testing. Figure 8 shows samples from each class of the BreakHis dataset.

4.3. Description of Experiments

We have carried out three types of experiments to evaluate the proposed BiT descriptor: (i) experiments on texture images to evaluate invariance of the BiT descriptor to rotation and scale; (ii) experiments on texture images in which the accuracy of classification algorithms trained using BiT descriptors extracted from images are computed for a comparative analysis with traditional texture descriptors; (iii) experiments on HIs in which sensitivity, specificity, and Kappa scores are computed as quantitative measures. Such measures are frequently used in medical imaging.
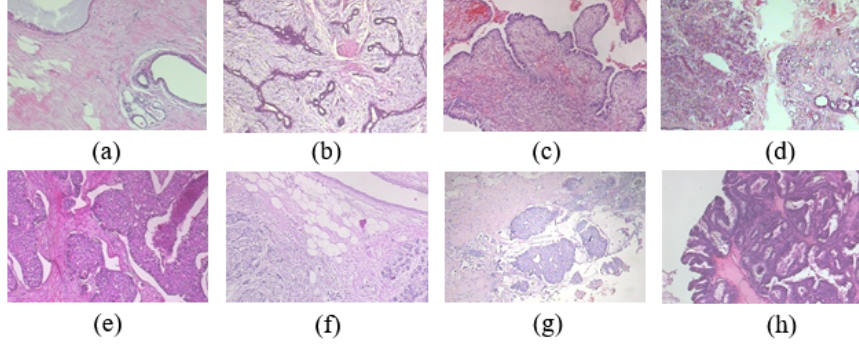
Figure 8: Example of HIs: (a) Adenosis, (b) Fibroadenoma, (c) Phyllodes, (d) Tabular adenomaa, (e) Ductal carcinoma, (f) Lobular carcinoma, (g) Mucinous carcinoma, (h) Papillary carcinoma, where (a) to (d) are benign and (e) to (f) are malignant tumors.

The invariance properties of the proposed BiT descriptors are evaluated on different transformations applied to texture images. We compute the BiT descriptors for each image and compare them to those computed from the transformed images. In this case, feature values should not change with the transformations.

The BiT descriptor is evaluated by the accuracy achieved on three texture datasets when used to extract features. Different classification algorithms are trained with such a feature vector. The same classification algorithms are trained with other texture descriptors, and their performance is compared with the performance achieved with BiT. For a fair comparison with other texture descriptors, we use the same approach described in Section 3 for all texture descriptors. Furthermore, the feature extraction procedure described in Algorithm 1, was also used for all texture descriptors. We have used SVM and k-NN and four ensemble learning algorithms: decision tree-based ensemble algorithm that uses a gradient boosting framework (XGBCB), a histogram-based algorithm for building gradient boosting ensembles of decision trees (HistoB), light gradient boosting decision trees (LightB), and super learner (SuperL) [59], which involves the selection of different base classifiers and the evaluation of their performances using a resampling technique. SuperL applies a stacked generalization through out-of-fold predictions during k-fold cross-validation. The base classifiers used in SuperL are k-NN, decision trees, and ensembles of decision trees such as adaboost, bagging, extra trees, and random forest.

The BiT descriptor is also evaluated by the accuracy, specificity, sensitivity, and Kappa score achieved on two HI datasets. In this case, only the classification algorithm that achieved the best performance with BiT is retained, and its performance is compared with the state-of-the-art of these datasets, which includes CNNs. These experiments are performed using a stratified k-fold

19

cross-validation.

5. Results and Discussion

5.1. Invariance of the BiT Descriptor

Figure 9 illustrates different transformations of texture images (first row) and HIs (second row). For each image, we have computed some BiT descriptors from each transformation and non-normalized feature values are presented in Tables 1 and 2.
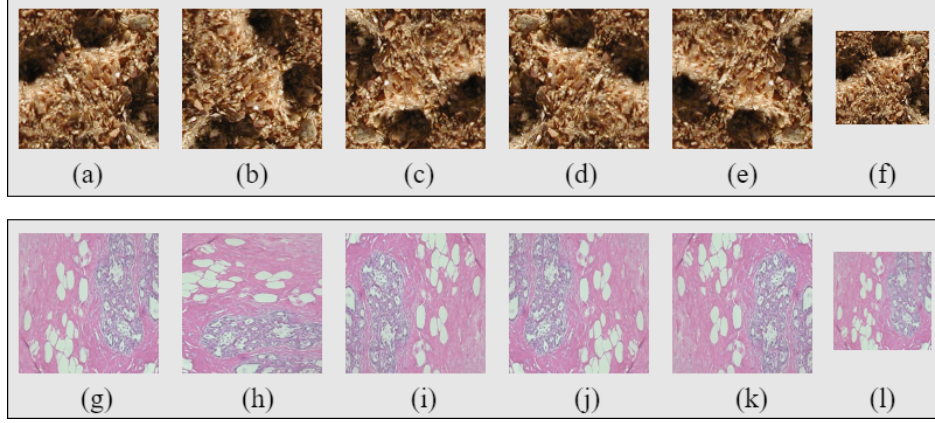

Figure 9: Example of texture image: (a) Original image, (b) rotation 90°, (c) rotation 180°, (d) Horizontal reflection, (e) Vertical reflection, (f) rescaled 50%. Example of histopathologic image: (g) Original image, (h) rotation 90°, (i) rotation 180°, (j) Horizontal reflection, (k) Vertical reflection, (l) rescaled 50%.

The values of BiT descriptors presented in Tables 1 and 2 show that: (i) all measurements employed are invariant to rotation and reflection as shown in Figures 9(a)-(e) and 9(g)-(k), since they presented the same values for all texture images or HIs. This also corroborates the fact that BiT descriptors capture the all-inclusive behaviors of patterns in an image; (ii) Shannon-Wiener diversity index (d_{SW}), taxonomic distinctness (Δ^*), intensive quadratic entropy (e_{IQ}), and the average distance from the nearest neighbor (d_{NN}) are invariant to scale as they provided values of the order of other transformations for each of the images. On the other hand, the measures based on richness and abundance show some dependence to scale. By changing the image scale, we somehow affect the proportion of both factors, which affects the resulting values either directly or inversely. However, this may be somehow compensated by normalizing such measures by the total number of pixels. On the other hand, taxonomic indices rely on the parenthood relationship between species. They are not affected by the change in scale, as the phylogenetic relationship depends on the intrinsic proprieties found in the ecosystem (image).

Table 1: Non-normalized feature values computed from different image transformations applied to a texture image 9(a).

| BiT Features | Original | Transformations | | | | |
| | | Rotation | | Reflection | | Rescaling |
		90°	180°	Horizontal	Vertical	50%
d_{Mg}	2636.49	2636.49	2636.49	2636.49	2636.49	725.45
e_M	0.00055	0.00055	0.00055	0.00055	0.00055	0.00109
d_{Mn}	20.3073	20.3073	20.3073	20.3073	20.3073	10.1634
d_{SW}	15.0453	15.0453	15.0453	15.0453	15.0453	14.9963
Δ	101297.7	101297.7	101297.7	101297.7	101297.7	6253.41
Δ^*	2.002325	2.002325	2.002325	2.002325	2.002325	2.003482
e_{IQ}	2.4900637	2.4900637	2.4900637	2.4900637	2.4900637	2.4901419
d_{NN}	4.9999	4.9999	4.9999	4.9999	4.9999	4.9999

Table 2: Non-normalized feature values computed from different image transformations applied to a histopathologic image 9(g).

| BiT Features | Original | Transformations | | | | |
| | | Rotation | | Reflection | | Rescaling |
		90°	180°	Horizontal	Vertical	50%
d_{Mg}	1975.95	1975.95	1975.95	1975.95	1975.95	548.347
e_M	0.00036	0.00036	0.00036	0.00036	0.00036	0.00072
d_{Mn}	13.2022	13.2022	13.2022	13.2022	13.2022	6.64831
d_{SW}	14.8910	14.8910	14.8910	14.8910	14.8910	14.6985
Δ	214389.7	214389.7	214389.7	214389.7	214389.7	15287.596
Δ^*	2.00673	2.00673	2.00673	2.00673	2.00673	2.00710
e_{IQ}	2.48115	2.48115	2.48115	2.48115	2.48115	2.48099
d_{NN}	4.9998	4.9998	4.9998	4.9998	4.9998	4.9998

5.2. Experiments with Texture Datasets

Table 3 shows the accuracy achieved by monolithic classifiers and ensemble methods on four texture descriptors: LBP, GLCM, Haralick, and BiT. The proposed BiT descriptor provided the best accuracy for most of the classification algorithms, and the best result was achieved with BiT and SuperL (96.34%), which outperformed all texture descriptors. The difference in accuracy achieved by BiT and the second and the third-best texture descriptors (Haralick+k-NN and GLCM+k-NN) are nearly 5% and 13%, respectively.

Table 3: accuracy (%) on the test set of Salzburg dataset. The best results are in boldface.

| Texture Descriptors | Classification Algorithms | | | | | |
	XGBCB	HistoB	LightB	SuperL	k-NN	SVM
LBP	57.10±0.024	58.80±0.029	55.10±0.021	64.06	33.61	61.58
GLCM	79.20±0.022	81.20±0.018	80.70±0.016	79.17	82.20	73.97
Haralick	86.10±0.015	88.20±0.017	89.60±0.017	90.19	**90.30**	89.92
BiT	**89.71±0.015**	**90.31±0.014**	**92.68±0.013**	**96.34**	88.36	**94.71**

A direct comparison of the results presented in Table 3 with other works may not be reasonable owing to differences in the experimental protocols. For example, the subclasses used in the experiments are not clearly specified as well as the samples in the test set.

Table 4 shows the accuracy achieved by monolithic classifiers and ensemble methods on four texture descriptors: LBP, GLCM, Haralick, and BiT. The proposed BiT descriptor provided the best accuracy for all classification algorithms, and BiT+SVM (100%) achieved the best result, which outperformed all texture descriptors. The difference in accuracy achieved by BiT and the second and the third-best texture descriptors (Haralick+SupeL and GLCM+SuperL) are nearly 7% and 8%, respectively.

Table 4: Accuracy (%) on the test set of Outex dataset. Best results are in bold face.

Texture	Classification Algorithms					
Descriptors	XGBCB	HistoB	LightB	SuperL	k-NN	SVM
LBP	54.90±0.011	58.90±0.013	56.60±0.014	81.02	46.40	81.41
GLCM	90.30±0.007	90.80±0.005	92.60±0.006	93.42	91.30	92.40
Haralick	92.40±0.003	92.40±0.003	92.20±0.004	93.81	92.90	93.40
BiT	**99.20±0.006**	**99.30±0.005**	**99.30±0.006**	**99.35**	**99.10**	**100.00**

Several works have also used the Outex dataset for texture classification. Although a direct comparison is not possible due to differences in the experimental protocols, Mehta and Egiazarian [60] presented an approach based on dominant rotated LBP, which achieved an accuracy of 96.26% with a k-NN. The approach is rotation invariant. Nonetheless, it has a downside of not considering color information and global features. Du et al. [61] presented an approach based on a local spiking pattern. This approach has the advantage of being rotation invariant, impulse noise resistant, and illumination invariant. Notwithstanding, it is not extended for color textures, and many input parameters are required. They achieved an accuracy of 86.12% with a neural network. Finally, Table 5 shows the accuracy achieved by monolithic classifiers and ensemble methods on four texture descriptors: LBP, GLCM, Haralick, and BiT. The proposed BiT descriptor provided the best accuracy for four out of six classification algorithms. However, BiT+SVM (98.93%) achieved the best result, which outperformed all texture descriptors.

The difference in accuracy achieved by BiT and the second and the third-best texture descriptors (Haralick+SVM and GLCM+SVM) are nearly 5% and 11%. Nonetheless, the Haralick descriptor presented an equal and slightly higher accuracy than BiT for XGBCB and HistoB ensemble methods, respectively.

Table 5: Accuracy (%) on the test set of KTH-TIPS dataset. Best results are in bold face.

Texture Descriptors	Classification Algorithms					
	XGBCB	HistoB	LightB	SuperL	k-NN	SVM
LBP	59.11±0.021	61.83±0.031	57.15±0.019	65.32	59.61	62.48
GLCM	86.20±0.028	88.10±0.017	87.10±0.022	86.21	84.81	87.90
Haralick	**92.20±0.019**	**93.90±0.019**	93.00±0.020	90.15	92.84	94.29
BiT	92.00±0.024	92.80±0.022	**93.30±0.024**	**96.07**	**95.46**	**98.93**

The KTH-TIPS dataset has also been used to evaluate approaches for texture classification. Even if a direct comparison may not be reasonable due to differences in the experimental protocols, Mehta and Egiazarian [60] also evaluated their approach on such a dataset and achieved an accuracy of 96.78% with k-NN. Hazgui et al. [62] presented an approach based on genetic programming and fusion of HOG and LBP features. Such an approach achieved an accuracy of 91.20% with a k-NN. Nevertheless, it does not consider color information and global features. Moreover, Nguyen et al. [63] presented statistical binary patterns, which are rotational and noise invariant. Such an approach reached an accuracy of 97.73%, which is 1.3% lower than the accuracy achieved by BiT+SVM. However, in addition to being resolution sensitive, this method presents a high computational complexity. Despite differences in the experimental protocol Qi et al. [28] studied the relative variance of texture patterns between different channels through LBP, as feature descriptor, and Shannon entropy to encode the cross-channel texture correlation. Therefore, they proposed a multi-scale cross-channel LBP (CCLBP), which is rotation-invariant. The CCLBP first computes the LBP descriptors in each channel and for each scale (total of 3 scales), afterward conducts the co-occurrence statistics, and the extracted features are concatenated. Such an approach achieved an accuracy of 99.01% for three scales with an SVM, which is 0.17% higher than the accuracy achieved by BiT+SVM. Notwithstanding, scale invariance, for example, is not an advantage provided by this method.

5.3. Experiments with HI datasets

Table 6 shows the accuracy achieved by monolithic classifiers and ensemble methods trained with BiT descriptors on the CRC dataset. Among all classification algorithms, SuperL provided the best results. We have also computed other important metrics used in medical images for BiT+SuperL. Specificity, sensitivity, and Kappa achieved on the CRC dataset are 94.43%, 94.47%, and 93.87%, respectively. Table 7 compares the results achieved by BiT+SuperL with the state-of-the-art for the CRC dataset. The proposed descriptor outperforms slightly the accuracy achieved

by all other methods. The difference in accuracy to the second-best method (CNN) is 0.56%, considering an 8-class classification task.

It is worthy of mention that the success of CNNs relies on the ability to leverage massive labeled datasets to learn high-quality representations. They have been widely employed on different image classification tasks due to their discriminative capability. Considering that they learn iteratively, a large amount of data is required to train CNNs to obtain desired results. Notwithstanding, data availability for a few fields may be scanty, and therefore CNNs become prohibitive in several domains. This is the case in medical imaging. The results achieved by the BiT descriptor on the CRC dataset for HI classification have shown that the proposed descriptor works well on other types of images, which have other structures than textures, with no need for data augmentation.

Table 6: Accuracy (%) of monolithic classifiers and ensemble methods with BiT descriptor on CRC dataset.

Texture	Classification Algorithms					
Descriptor	XGBCB	HistoB	LightB	SuperL	k-NN	SVM
BiT	91.00±0.009	91.80±0.010	91.20±0.011	**92.96**	88.10	91.45

Table 7: Average accuracy (%) of shallow and deep approaches on the CRC dataset.

Reference	Approach	10-fold	5-fold
Ribeiro et al. [64]	Shallow	97.60*	–
Kather et al. [65]	Shallow	87.40	–
Sarkar and Acton [66]	Shallow	73.60	–
BiT+SuperL	Shallow	**92.96**	–
Wang et al. [67]	CNN	–	92.60
Pham [68]	CNN	–	84.00
Raczkowski et al. [69]	CNN	92.40	92.20

*Used 2-classes classification instead.

Table 8 shows the accuracy achieved by monolithic classifiers and ensemble methods trained with BiT descriptor on the BreakHis dataset. The SVM classifier achieved the best accuracy for all magnifications, followed by Super Learner. Table 9 shows specificity, sensitivity, and Kappa achieved by BiT and SVM. Table 10 compares the results achieved by BiT+SVM with the state-of-the-art for the BreakHis dataset. The proposed descriptor achieved a considerable accuracy of 97.50% for 40× magnification, which slightly outperforms the accuracy of both shallow and deep methods. The difference in accuracy between the proposed method and the second-best method (CNN) is about 0.5% for 40× magnification. Notwithstanding, the best CNN method outperforms BiT for 100×, 200×, and 400× magnification with difference of 0.70%, 1.40% and

2.00%, respectively. Moreover, Table 10 presents the results achieved by Spanhol et al. [58], which also used LBP, GLCM, and other texture descriptors with monolithic classifiers and ensemble methods. For instance, the results achieved by BiT+SVM outperform their GLCM approach by 22.8%, 20.0%, 12.4% and 13.5% for $40\times$, $100\times$, $200\times$ and $400\times$, respectively.

Table 8: Accuracy (%) of classification algorithms on the test set of the BreakHis dataset.

Classification	Magnification			
Algorithms	$40\times$	$100\times$	$200\times$	$400\times$
XGBCB	94.55	94.85	93.36	90.51
HistoB	94.25	95.38	93.86	91.45
LightB	94.39	94.95	92.61	90.10
SuperL	96.61	95.72	93.57	93.86
SVM	**97.50**	**96.80**	**95.80**	**95.20**

Table 9: Specificity, sensitivity, and Kappa for BiT+SVM on the test set of the BreakHis dataset.

Magnification	Specificity	Sensitivity	Kappa
$40\times$	95.77	95.75	95.14
$100\times$	95.27	95.28	95.09
$200\times$	94.39	94.38	93.45
$400\times$	94.49	94.46	93.50

Table 10: Accuracy (%) of shallow and deep approaches on the BreakHis dataset. All these works used the same data partitions for training and test.

Reference	Method	$40\times$	$100\times$	$200\times$	$400\times$
Spanhol et al. [58]*	Shallow	75.60	73.00	72.90	71.20
Spanhol et al. [58]+	Shallow	74.70	76.80	83.40	81.70
Erfankhah et al. [70]	Shallow	88.30	88.30	87.10	83.40
BiT+SVM	Shallow	**97.50**	96.80	95.80	95.20
Alom et al. [71]	CNN	97.00	**97.50**	**97.20**	**97.20**
Han et al. [72]	CNN	92.80	93.90	93.70	92.90
Bayramoglu et al. [73]	CNN	83.00	83.10	84.60	82.10
Spanhol et al. [74]	CNN	90.00	88.40	84.60	86.10

*: LBP; +: GLCM.

Even if CNNs have overcome shallow methods for several classification tasks, their advantages on texture images are not so high. CNNs must be trained on large amounts of data, and they often require retraining or fine-tuning some of their layers to deal with different problems. Besides that, CNNs are complex and usually have thousands of trainable parameters demanding extensive computational resources for training such models. In contrast, the computation of BiT descriptors is relatively very low. Furthermore, the proposed BiT descriptor is generic. It does not require

retraining or hyperparameter configuration while providing state-of-the-art performance, as shown in the experimental results over different datasets.

6. Conclusions

This paper has presented an important contribution to texture characterization using biodiversity measurements and taxonomic distinctiveness. We have proposed a bio-inspired texture descriptor named BiT, which is based on abstract modeling of an ecosystem as a gray-level image where image pixels correspond to a community of organisms. We have revisited several biodiversity measurements and taxonomic distinctiveness to compute features based on species richness, species abundance, and taxonomic indices. The combination of species richness, species abundance, and taxonomic indices takes advantage of the invariance characteristics of ecological patterns such as reflection, rotation, and scale.

These bio-inspired features form a robust and invariant texture descriptor that can be used together with machine learning algorithms to build classification models. Experimental results on texture and HI datasets have shown that the proposed texture descriptor can train different classification algorithms that outperformed traditional texture descriptors and achieved very competitive results compared to deep methods. Therefore, the proposed texture descriptor is promising for mainly dealing with texture analysis and characterization problems. The results demonstrate the promising performance of such a bio-inspired texture descriptor presented.

Considering that the image channels are separated and that the features are extracted using the same measures, it is possible to have redundant and irrelevant features, which may affect the classification performance. This issue opens the door for a feature selection step. Thus, as future work, we intend to integrate a decision-maker-based multi-objective feature selection into the feature extraction procedure to find a solution that makes a trade-off between the number of features and accuracy.

26

References

[1] M. Pietikäinen, T. Mäenpää, J. Viertola, Color texture classification with color histograms and local binary patterns, in: Workshop on Texture Analysis in Machine Vision, volume 1, 2002.

[2] J. R. Bergen, E. H. Adelson, Early vision and texture perception, Nature 333 (1988) 363–364.

[3] J. Hu, D. Li, Q. Duan, Y. Han, G. Chen, X. Si, Fish species classification by color, texture and multi-class support vector machine using computer vision, Computers and Electronics in Agriculture 88 (2012) 133–140.

[4] G. Zhao, M. Pietikainen, Dynamic texture recognition using local binary patterns with an application to facial expressions, IEEE Trans on Pattern Analysis and Machine Intelligence 29 (2007) 915–928.

[5] F. S. Khan, J. Van De Weijer, M. Vanrell, Top-down color attention for object recognition, in: IEEE 12th Int'l Conf on Computer Vision, 2009, pp. 979–986.

[6] S. H. Ong, X. C. Jin, R. Sinniah, et al., Image analysis of tissue sections, Computers in Biology and Medicine 26 (1996) 269–279.

[7] Y. Costa, L. Oliveira, A. L. Koerich, F. Gouyon, Music genre recognition using Gabor filters and LPQ texture descriptors, in: Iberoamerican Congress on Pattern Recognition, Springer, 2013, pp. 67–74.

[8] J. Li, W. Rich, D. Buhl-Brown, Texture analysis of remote sensing imagery with clustering and bayesian inference, Int'l J. Image Graphics Signal Processing 7 (2015) 1–10.

[9] W. Li, M. Fritz, Recognizing materials from virtual examples, in: European Conf on Computer Vision, Springer, 2012, pp. 345–358.

[10] D. Vriesman, A. de Souza Britto Jr., A. Zimmer, A. L. Koerich, R. Paludo, Automatic visual inspection of thermoelectric metal pipes, Signal Image Video Process. 13 (2019) 975–983.

[11] M. Tuceryan, A. K. Jain, Texture analysis, in: Handbook of Pattern Recognition and Computer Vision, World Scientific, 1993, pp. 235–276.

[12] R. M. Haralick, K. Shanmugam, I. Dinstein, Textural features for image classification, IEEE Trans on Systems, Man, and Cybernetics (1973) 610–621.

[13] R. M. Haralick, Statistical and structural approaches to texture, Proc. of the IEEE 67 (1979) 786–804.

[14] M. Pietikäinen, A. Hadid, G. Zhao, T. Ahonen, Computer vision using local binary patterns, volume 40, Springer Science & Business Media, 2011.

[15] S. Arivazhagan, L. Ganesan, Texture classification using wavelet transform, Pattern Recognition Letters 24 (2003) 1513–1521.

[16] G. R. Cross, A. K. Jain, Markov random field texture models, IEEE Trans on Pattern Analysis and Machine Intelligence (1983) 25–39.

[17] I. Fogel, D. Sagi, Gabor filters as texture discriminator, Biological Cybernetics 61 (1989) 103–113.

[18] V. Ojansivu, J. Heikkilä, Blur insensitive texture classification using local phase quantization, in: Int'l Conf on Image and Signal Processing, 2008, pp. 236–243.

[19] J. Saxena, K. Teckchandani, P. Pandey, M. K. Dutta, C. M. Travieso, J. B. Alonso-Hernández, et al., Palm vein recognition using local tetra patterns, in: 4th Int'l Conf on Bioinspired Intelligence, 2015, pp. 151–156.

[20] J. Kannala, E. Rahtu, Bsif: Binarized statistical image features, in: 21st Int'l Conf on Pattern Recognition, 2012, pp. 1363–1366.

[21] L. M. Kaplan, Extended fractal analysis for texture classification and segmentation, IEEE Trans on Image Processing 8 (1999) 1572–1585.

[22] P. Simon, V. Uma, Review of texture descriptors for texture classification, in: Data Engineering and Intelligent Computing, Springer, 2018, pp. 159–176.

[23] L. Liu, J. Chen, P. Fieguth, G. Zhao, R. Chellappa, M. Pietikäinen, From bow to cnn: Two decades of texture representation for texture classification, Int'l Journal of Computer Vision 127 (2019) 74–109.

[24] V. Andrearczyk, P. F. Whelan, Using filter banks in convolutional neural networks for texture classification, Pattern Recognition Letters 84 (2016) 63–69.

[25] J. de Matos, A. de Souza Britto Jr., L. E. S. de Oliveira, A. L. Koerich, Texture CNN for histopathological image classification, in: 32nd IEEE Int'l Symp on Computer-Based Medical Systems, 2019, pp. 580–583. doi:10.1109/CBMS.2019.00120.

[26] S. Fujieda, K. Takayama, T. Hachisuka, Wavelet convolutional neural networks for texture classification, arXiv preprint arXiv:1707.07394 (2017).

[27] D. Vriesman, A. S. Britto Junior, A. Zimmer, A. L. Koerich, Texture CNN for thermoelectric metal pipe image classification, in: IEEE 31st Int'l Conf on Tools with Artificial Intelligence, 2019, pp. 569–574. doi:10.1109/ICTAI.2019.00085.

[28] X. Qi, Y. Qiao, C. Li, J. Guo, Exploring cross-channel texture correlation for color texture classification, in: T. Burghardt, D. Damen, W. W. Mayol-Cuevas, M. Mirmehdi (Eds.), British Machine Vision Conf, 2013. doi:10.5244/C.27.97.

[29] C. B. Nsimba, A. L. Levada, Exploring information theory and gaussian markov random fields for color texture classification, in: Int'l Conf on Image Analysis and Recognition, Springer, 2020, pp. 130–143.

[30] L. M. Azevedo, J. D. S. de Almeida, J. D. S. de Almeida, A. C. de Paiva, A. C. de Paiva, G. Braz Júnior, R. MS Veras, Diagnóstico de glaucoma em retinografias usando índices taxonômicos e aprendizado de máquina, Revista de Sistemas e Computação 10 (2020).

[31] A. O. de Carvalho Filho, A. C. Silva, A. C. de Paiva, R. A. Nunes, M. Gattass, Lung-nodule classification based on computed tomography using taxonomic diversity indexes and an svm, Journal of Signal Processing Systems 87 (2017) 179–196.

[32] A. E. Magurran, Measuring Biological Diversity, Blackwell Publishing, 2004.

[33] R. Rousseau, P. Van Hecke, D. NIjssen, J. Bogaert, The relationship between diversity profiles, evenness and species richness based on partial ordering, Environmental and Ecological Statistics 6 (1999) 211–223.

[34] K. R. Clarke, R. M. Warwick, A taxonomic distinctness index and its statistical properties, Journal of Applied Ecology 35 (1998) 523–531.

[35] C. Sohier, Measurements of biodiversity, `http://www.coastalwiki.org/wiki/Measurements_of_biodiversity`, 2019.

[36] L. Jost, Partitioning diversity into independent alpha and beta components, Ecology 88 (2007) 2427–2439.

[37] SDR-IV, Species diversity and richness 4, `http://www.pisces-conservation.com/sdrhelp/index.html?bergerparker.htm`, 2020.

[38] H. T. Clifford, W. Stephenson, et al., An introduction to numerical classification, volume 240, Academic Press New York, 1975.

[39] R. H. Whittaker, Evolution and measurement of species diversity, Taxon 21 (1972) 213–251.

[40] R. M. May, M. Cody, J. M. Diamond, Ecology of species and communities (1975).

[41] R. A. Fisher, A. S. Corbet, C. B. Williams, The relation between the number of species and the number of individuals in a random sample of an animal population, The Journal of Animal Ecology (1943) 42–58.

[42] R. A. Kempton, L. R. Taylor, Models and statistics for species diversity, Nature 262 (1976) 818–820.

[43] C. Heip, P. Engels, Comparing species diversity and evenness indices, Journal of the Marine Biological Association of the United Kingdom 54 (1974) 559–563.

[44] S. I. Rogers, K. R. Clarke, J. D. Reynolds, The taxonomic distinctness of coastal bottom-dwelling fish communities of the north-east atlantic, Journal of Animal Ecology 68 (1999) 769–782.

[45] R. Gibson, M. Barnes, R. Atkinson, Practical measures of marine biodiversity based on relatedness of species, Oceanography and Marine Biology 39 (2001) 207–231.

[46] J. Izsáki, L. Papp, Application of the quadratic entropy indices for diversity studies of drosophilid assemblages, Environmental and Ecological Statistics 2 (1995) 213–224.

[47] S. Pavoine, S. Ollier, A.-B. Dufour, Is the originality of a species measurable?, Ecology Letters 8 (2005) 579–586.

[48] D. P. Faith, Conservation evaluation and phylogenetic diversity, Biological Conservation 61 (1992) 1–10.

[49] M. Vellend, W. K. Cornwell, K. Magnuson-Ford, A. Ø. Mooers, Measuring phylogenetic biodiversity, Biological Diversity: Frontiers in Measurement and Assessment (2011) 194–207.

[50] C. Ricotta, A parametric diversity measure combining the relative abundances and taxonomic distinctiveness of species, Diversity and Distributions 10 (2004) 143–146.

[51] R. I. Vane-Wright, C. J. Humphries, P. H. Williams, What to protect?—systematics and the agony of choice, Biological Conservation 55 (1991) 235–254.

[52] S. A. Frank, J. Bascompte, Invariance in ecological pattern, F1000Research 8 (2019).

[53] A. J. Daly, J. M. Baetens, B. De Baets, Ecological diversity: measuring the unmeasurable, Mathematics 6 (2018) 119.

[54] R. Rousseau, P. Van Hecke, D. NIjssen, J. Bogaert, The relationship between diversity profiles, evenness and species richness based on partial ordering, Environmental and Ecological Statistics 6 (1999) 211–223.

[55] H. Shimadzu, M. Dornelas, P. A. Henderson, A. E. Magurran, Diversity is maintained by seasonal variation in species abundance, BMC Biology 11 (2013) 98.

[56] T. R. Crimmins, Geometric filter for speckle reduction, Applied Optics 24 (1985) 1438–1443.

[57] J. N. Kather, C.-A. Weis, F. Bianconi, S. M. Melchers, L. R. Schad, T. Gaiser, A. Marx, F. G. Zöllner, Multi-class texture analysis in colorectal cancer histology, Scientific Reports 6 (2016) 27988.

[58] F. A. Spanhol, L. S. Oliveira, C. Petitjean, L. Heutte, A Dataset for Breast Cancer Histopathological Image Classification, IEEE Trans on Biomedical Engineering 63 (2016) 1455–1462.

[59] M. J. van der Laan, E. C. Polley, A. E. Hubbard, Super learner, Statistical Applications in Genetics and Molecular Biology 6 (2007).

[60] R. Mehta, K. Egiazarian, Dominant rotated local binary patterns (DRLBP) for texture classification, Pattern Recognition Letters 71 (2016) 16–22.

[61] S. Du, Y. Yan, Y. Ma, Local spiking pattern and its application to rotation-and illumination-invariant texture classification, Optik 127 (2016) 6583–6589.

[62] M. Hazgui, H. Ghazouani, W. Barhoumi, Genetic programming-based fusion of HOG and LBP features for fully automated texture classification, The Visual Computer 37 (2021) 1–20.

[63] T. P. Nguyen, N.-S. Vu, A. Manzanera, Statistical binary patterns for rotational invariant texture classification, Neurocomputing 173 (2016) 1565–1577.

[64] M. G. Ribeiro, L. A. Neves, M. Z. do Nascimento, G. F. Roberto, A. S. Martins, T. A. A. Tosta, Classification of colorectal cancer based on the association of multidimensional and multiresolution features, Expert Systems with Applications 120 (2019) 262–278.

[65] J. N. Kather, C.-A. Weis, F. Bianconi, S. M. Melchers, L. R. Schad, T. Gaiser, A. Marx, F. G. Zöllner, Multi-class texture analysis in colorectal cancer histology, Scientific Reports 6 (2016) 27988.

[66] R. Sarkar, S. T. Acton, Sdl: Saliency-based dictionary learning framework for image similarity, IEEE Trans on Image Processing 27 (2017) 749–763.

[67] C. Wang, J. Shi, Q. Zhang, S. Ying, Histopathological image classification with bilinear convolutional neural networks, in: 39th Annual Int'l Conf of the IEEE Engineering in Medicine and Biology Society, 2017, pp. 4050–4053.

[68] T. D. Pham, Scaling of texture in training autoencoders for classification of histological images of colorectal cancer, in: Int'l Symposium on Neural Networks, Springer, 2017, pp. 524–532.

[69] Ł. Raczkowski, M. Możejko, J. Zambonelli, E. Szczurek, Ara: accurate, reliable and active histopathological image classification framework with bayesian deep learning, Scientific Reports 9 (2019) 1–12.

[70] H. Erfankhah, M. Yazdi, M. Babaie, H. R. Tizhoosh, Heterogeneity-aware local binary patterns for retrieval of histopathology images, IEEE Access 7 (2019) 18354–18367.

[71] M. Z. Alom, C. Yakopcic, M. S. Nasrin, T. M. Taha, V. K. Asari, Breast cancer classification from histopathological images with inception recurrent residual convolutional neural network, Journal of Digital Imaging 32 (2019) 605–617.

[72] Z. Han, B. Wei, Y. Zheng, Y. Yin, K. Li, S. Li, Breast cancer multi-classification from histopathological images with structured deep learning model, Scientific Reports 7 (2017) 1–10.

[73] N. Bayramoglu, J. Kannala, J. Heikkilä, Deep learning for magnification independent breast cancer histopathology image classification, in: 23rd Int'l Conf on Pattern Recognition, 2016, pp. 2440–2445.

[74] F. A. Spanhol, L. S. Oliveira, C. Petitjean, L. Heutte, Breast cancer histopathological image classification using convolutional neural networks, in: Int'l Joint Conf on Neural Networks, 2016, pp. 2560–2567.

Supplementary Material

All the libraries and implementations will be provided upon the acceptance of the paper in the following online public repository:

`https://github.com/stevetmat/BioInspiredFDesc`